25

Planar Defects

CHAPTER PREVIEW

Internal interfaces (grain boundaries, phase boundaries, stacking faults) or external interfaces (i.e., surfaces) are surely the most important defects in crystalline engineering materials. Their common feature is that we can usually think of them as all being two-dimensional, or planar, defects (even though they're not really). The main topics of this chapter will be

- Characterizing which type of internal interface we have and determining its main parameters.
- Identifying lattice translations at these interfaces from the appearance of the diffraction-contrast images.

Rotations are usually associated with line defects and they will be discussed in Chapter 26. We can't usually identify the details of the local structure of an interface unless we use HRTEM, so we will return to that topic in Chapter 28. We'll talk a little about simulating images of these defects because it is relatively direct and instructive.

25.1 TRANSLATIONS AND ROTATIONS

This section is a brief summary of some fundamentals of materials science. If the concepts are not immediately familiar to you, then go and study an introductory textbook on defects in materials, several of which are in the reference section.

An interface is simply a surface which separates any two distinct regions of the microstructure. For most of our discussion, we will make the assumption that the surface is flat and is thus a planar (parallel to a plane) defect, though this is rarely the case. We can sketch a general interface as shown in Figure 25.1

With this general definition, we can summarize the different classes of planar defects

- *Translation boundary, RB*. Any translation **R**(**r**) is allowed, θ is zero, and both regions are identical and thus perfectly aligned. Stacking faults (SFs) are a special case. We'll denote the translation boundary as RB so as to avoid confusing it with the twin boundary (TB).
- *Grain boundary, GB*. Any values of **R**(**r**), **n**, and θ are allowed (**n** is the normal to the defect plane), but the chemistry and structure of the two grains must be the same. The SF is again a special case, but this class also includes TBs.
- *Phase boundary, PB*. As for a GB, but the chemistry and/or structure of the two regions can differ.
- *Surface*. A special case of a PB where one phase is vacuum or gas.

DEFINE R(r)

The upper crystal is held fixed while the lower one is translated by a vector **R**(**r**) and/or rotated through some angle θ about any axis, **v**.

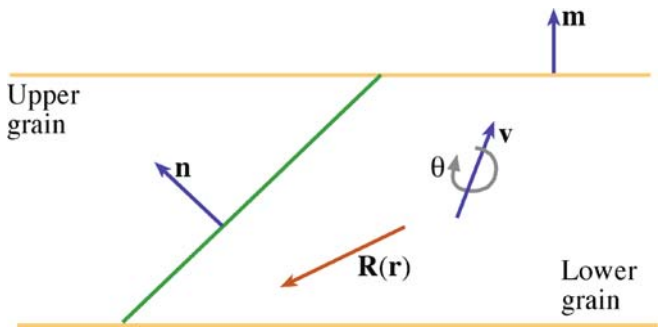

FIGURE 25.1. A specimen containing a planar defect. The lower grain is translated by a vector **R**(**r**), and rotated through an angle θ about the vector **v**, relative to the upper grain. The defect plane normal is **n**, the foil normal is **m**.

TABLE 25.1 Examples of Internal Planar Defects

Planar defect	Structure	Example	Example
SF	Diamond-cubic, fcc, zinc blende	Cu, Ag, Si, GaAs	$\mathbf{R} = \frac{1}{3}[111]$ or $\mathbf{R} = \frac{1}{6}[112]$
APB/IDB	Zinc blende, wurtzite	GaAs, AlN	Inversion
APB	CsCl	NiAl	$\mathbf{R} = \frac{1}{2}[111]$
APB/SF	Spinel	$MgAl_2O_4$	$\mathbf{R} = \frac{1}{4}[110]$
GB	All materials	Often denoted by Σ where Σ^{-1} is the fraction of coincident lattice sites	Rotation plus **R**
PB	Any two different materials	Sometimes denoted by Σ_1,Σ_2 which are not equal	Rotation plus **R** plus misfit
RB	Extra translation	{112} Twin boundary in Al	**R** not related to lattice

Now with each of these groups, we can have special examples. We will list some of the most common examples in Table 25.1, including those that we will consider in this chapter. For a more detailed discussion, we refer you to the general references at the end of the chapter.

RBs include the familiar SFs found in fcc, hcp, diamond-cubic, and layer materials. They have been widely studied because they play an important role in the mechanical properties of the fcc metals, e.g., Cu and stainless steel. They are also found in more complex materials such as spinels, Ni_3Al, Ti_3Al, etc., where the lattice parameters, and therefore the dislocation Burgers vectors, are large.

The anti-phase boundary (APB) in ordered CuAu (which we can describe as two interpenetrating simple-cubic superlattices) is produced by translating one superlattice by $\frac{1}{2}<111>$ with respect to the other. It is called an APB because one superlattice is out of phase with the other. If the crystal were disordered and the Cu and Au occupied the bcc sites randomly, then $\frac{1}{2}<111>$ would be a lattice vector and no defect would exist. This particular APB can thus be regarded as an SF. We will find that the methods used to characterize RBs can often be used to determine $\mathbf{R}(\mathbf{r})$ in other interfaces.

STACKING FAULT PLANES

Although we know that {111} is the favored SF plane for fcc metals, SFs in other materials lie on different planes.

GBs fall into two groups, low angle and high angle. Low-angle boundaries necessarily involve a rotation through a small angle that is usually accommodated by arrays of dislocations; we'll consider these defects in Chapter 26. High-angle boundaries can adopt some special values of **n** and θ; a large fraction of lattice sites in one grain is then shared by (is common to) the other grain. We characterize the fraction by the inverse of this fraction, which we call Σ. For example, the common twin boundary in fcc metals is the $\Sigma = 3$ grain boundary (the fraction is $\frac{1}{3}$). The reason this is important to our discussion is that if a set of lattice points is common to two grains (as implied by the Σ coincidence-site lattice concept), then certain planes may also be common and may give rise to common reflections. These reflections will remain common even if one grain is translated relative to the other. In that case, we'll have a special type of RB, called the rigid-body translation. Rigid-body translations in grain boundaries behave just like other SFs except **R** is usually small and is not directly related to the lattice parameters.

There is a second group of APBs where the two grains cannot be related by a translation. These occur in GaAs, ZnO, AlN, and SiC, for example. One lattice can always be related to the other by a rotation of 180° to give the equivalent of an inversion; they are sometimes known as inversion domain boundaries (IDBs). (They are $\Sigma = 1$ GBs.) These special interfaces can often be seen in the image because there is usually a small associated translation. We analyze this translation as if it were a simple RB because all the planes on one side of the IDB are parallel to their counterparts in the other; the (hkl) plane on one side is parallel to the $\bar{h}\bar{k}\bar{l}$ on the other. We can't distinguish **g** from $\bar{\mathbf{g}}$ unless we use CBED or we have a great specimen for HRTEM.

PBs are rarely (if ever) analyzed fully using diffraction contrast. If the orientation, chemistry, and structure can all change on crossing the boundary, then not only will the reflections change, but all extinction distances will change too. Some special examples of such interfaces are hcp-Co/fcc-Co, bcc-Fe/fcc-Fe, NiO/$NiFe_2O_4$, and $GaAs/Al_xGa_{1-x}As$. Of course, the number of other such interfaces is countless.

Surface studies using TEM have quite recently become very important although the experimental tools have been available for some time. We will discuss surfaces in this chapter insofar as they are imaged by diffraction contrast. So-called profile imaging will follow in Chapter 28 on HRTEM. The other two surface-sensitive techniques are plan-view and reflection electron microscopy (REM, see Chapter 29).

25.2 WHY DO TRANSLATIONS PRODUCE CONTRAST?

As usual, we will start our analysis considering only two beams, O and G. Our approach will use hand-waving arguments, which are not perfect, to justify adapting the Howie-Whelan equations for specimens containing interfaces. We'll use the same approach for other defects in Chapters 26 and 27. Because the Howie-Whelan equations for perfect crystals assume two-beam conditions, we are able to solve them analytically. We'd like to be able to do the same when defects are present, because this gives us a physical understanding of the processes which produce the contrast. There are two important features that we will need to keep in mind

- Diffraction contrast only occurs because we have Bloch waves in the crystal. However, our analysis will initially only consider diffracted beams.
- We make the column approximation so we can solve the equations; we must be wary whenever the specimen or the diffraction conditions change within a distance comparable to the column diameter.

TEM OF SURFACES
The techniques are (i) profile imaging, (ii) plan-view imaging, and (iii) reflection electron microscopy (REM).

A unit cell in a strained crystal will be displaced from its perfect-crystal position so that it is located at position $\mathbf{r}'_n$ instead of $\mathbf{r}_n$ where n is included to remind us that we are considering scattering from an array of unit cells; we'll soon omit the n (and we still have the column approximation)

$$\mathbf{r}'_n = \mathbf{r}_n + \mathbf{R}_n \tag{25.1}$$

In this expression, $\mathbf{R}_n$ is actually $\mathbf{R}_n(\mathbf{r})$; it can vary throughout the specimen. The term $e^{2\pi i\mathbf{K}.\mathbf{r}}$ in equation 13.3 (it's actually $\mathbf{Kr_n}$) now becomes $e^{2\pi i\mathbf{K}.\mathbf{r}'}$ so we need to examine the term $\mathbf{K}.\mathbf{r}'$. We know that $\mathbf{K}$ is $\mathbf{g} + \mathbf{s}$, so we can write

$$\mathbf{K}.\mathbf{r}'_n = (\mathbf{g}+\mathbf{s}).(\mathbf{r}_n+\mathbf{R}_n) = \mathbf{g}.\mathbf{r}_n + \mathbf{g}.\mathbf{R}_n + \mathbf{s}.\mathbf{r}_n + \mathbf{s}.\mathbf{R}_n \tag{25.2}$$

Now since $\mathbf{r}_n$ is a lattice vector, $\mathbf{g}.\mathbf{r}_n$ is an integer as usual. The third term, $\mathbf{s}.\mathbf{r}_n$ gives our usual sz term so the new terms are $\mathbf{g}.\mathbf{R}_n$ and $\mathbf{s}.\mathbf{R}_n$.

When we discuss strong-beam images we know that $\mathbf{s}$ is very small. Since we are using elasticity theory $\mathbf{R}_n$ must be small. Hence we ignore the term $\mathbf{s}.\mathbf{R}_n$. Remember that we have made a special assumption which may not be valid in two situations

- When $\mathbf{s}$ is large; we'll encounter this when we discuss the weak-beam technique in Chapter 27.
- When the lattice distortion, $\mathbf{R}$, is large; this occurs close to the cores of some defects.

We now modify equation 13.8 intuitively to include the effect of adding a displacement from equation 25.2

$$\frac{d\phi_{\mathbf{g}}}{dz} = \frac{\pi i}{\xi_{\mathbf{0}}}\phi_{\mathbf{g}} + \frac{\pi i}{\xi_{\mathbf{g}}}\phi_{\mathbf{0}}\exp[-2\pi i(sz + \mathbf{g}.\mathbf{R})] \tag{25.3}$$

and

$$\frac{d\phi_{\mathbf{0}}}{dz} = \frac{\pi i}{\xi_{\mathbf{0}}}\phi_{\mathbf{0}} + \frac{\pi i}{\xi_{\mathbf{g}}}\phi_{\mathbf{g}}\exp[+2\pi i(sz + \mathbf{g}.\mathbf{R})] \tag{25.4}$$

Next, we simplify these equations just as we did in Chapter 13 by setting

$$\phi_{\mathbf{0}}(z)_{(\mathrm{sub})} = \phi_{\mathbf{0}}\exp\left(\frac{-\pi i z}{\xi_{\mathbf{0}}}\right) \tag{25.5}$$

and

$$\phi_{\mathbf{g}}(z)_{(\mathrm{sub})} = \phi_{\mathbf{g}}\exp\left(2\pi i s z - \frac{\pi i z}{\xi_{\mathbf{0}}}\right) \tag{25.6}$$

Then the Howie-Whelan equations become

$$\frac{d\phi_{\mathbf{0}(\mathrm{sub})}}{dz} = \frac{\pi i}{\xi_{\mathbf{g}}}\phi_{\mathbf{g}(\mathrm{sub})}\exp(2\pi i\mathbf{g}.\mathbf{R}) \tag{25.7}$$

and

$$\frac{d\phi_{\mathbf{g}(\mathrm{sub})}}{dz} = \frac{\pi i}{\xi_{\mathbf{g}}}\phi_{\mathbf{0}(\mathrm{sub})}\exp(-2\pi i\mathbf{g}.\mathbf{R}) + 2\pi i s\phi_{\mathbf{g}(\mathrm{sub})} \tag{25.8}$$

These equations are just as before (equations 13.14 and 13.15) but with the addition of the $2\pi i\mathbf{g}.\mathbf{R}$ term. This additional phase is termed α, hence planar defects are seen when $\alpha \neq 0$.

$$\alpha = 2\pi\mathbf{g}.\mathbf{R} \tag{25.9}$$

These expressions will be particularly useful in two cases

- When $\mathbf{R}$ = constant.
- Understanding phasor diagrams when defects are present.

We start with a simple stacking fault lying parallel to the surface as shown in Figure 25.2. In this situation, the beams propagate through the upper layer just as if no fault were present. At a depth $z = t_1$, the beams may experience a phase change due to the effect of the

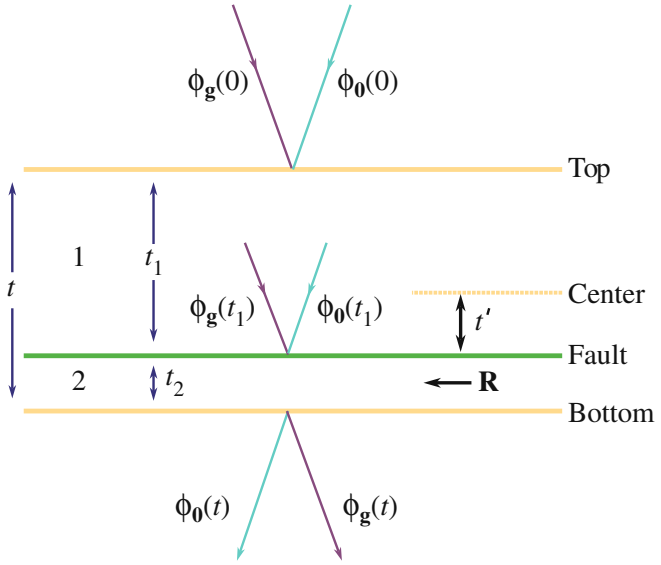

FIGURE 25.2. A stacking fault lying at depth t_1 in a parallel-sided uniformly thick specimen. The total thickness is t and $t_2 = t - t_1$.

translation **R**, but after that they again propagate as if in perfect crystal.

In this chapter, we'll see several values of α. A special case occurs when $\alpha = \pm 120°$. This value of α is often encountered since it occurs for fcc SFs. We'll also encounter the case where $\alpha = \pm 180°$; this value arises for some special APBs which are really SFs.

25.3 THE SCATTERING MATRIX

This discussion of the scattering matrix introduces no new concepts. It is just a different way of writing the equations so that if you are calculating the image contrast, you can program the computer more easily, especially when you have complicated arrays of lattice defects. Our reason for delaying the introduction of the scattering matrix until now is that it is much easier to understand when you can apply it to a specific problem.

In equations 13.17–13.20, we showed that in the two-beam case, we can write these simple expressions for ϕ_0 and ϕ_g

$$\phi_0 = C_0 e^{2\pi i \gamma z} \tag{25.10}$$

and

$$\phi_g = C_g e^{2\pi i \gamma z} \tag{25.11}$$

Since there are two values for γ, we can express both the **0** and **g** beams as the combination of these two contributions to give

$$\phi_0(z) = C_0^{(1)}\psi^{(1)} \exp\left(2\pi i \gamma^{(1)} z\right) + C_0^{(2)}\psi^{(2)} \exp\left(2\pi i \gamma^{(2)} z\right) \tag{25.12}$$

and

$$\phi_g(z) = C_g^{(1)}\psi^{(1)} \exp\left(2\pi i \gamma^{(1)} z\right) + C_g^{(2)}\psi^{(2)} \exp\left(2\pi i \gamma^{(2)} z\right) \tag{25.13}$$

where the $\psi^{(i)}$ terms tell us the relative contributions of the $\gamma^{(1)}$ and $\gamma^{(2)}$ terms. (We are really saying that both Bloch waves contribute to both the **0** and **g** beams.) We can rewrite equations 25.12 and 25.13 in a matrix form. (This is the key step.)

$$\begin{pmatrix} \phi_0(z) \\ \phi_g(z) \end{pmatrix} = \begin{pmatrix} C_0^{(1)} & C_0^{(2)} \\ C_g^{(1)} & C_g^{(2)} \end{pmatrix} \begin{pmatrix} \exp(2\pi i \gamma^{(1)} z) & 0 \\ 0 & \exp(2\pi i \gamma^{(2)} z) \end{pmatrix} \begin{pmatrix} \psi^{(1)} \\ \psi^{(2)} \end{pmatrix} \tag{25.14}$$

We can express our boundary conditions as

$$C_0^{(1)}\psi^{(1)} + C_0^{(2)}\psi^{(2)} = \phi_0(0) \tag{25.15}$$

and

$$C_g^{(1)}\psi^{(1)} + C_g^{(2)}\psi^{(2)} = \phi_g(0) \tag{25.16}$$

which we can now rewrite as

$$\begin{pmatrix} C_0^{(1)} & C_0^{(2)} \\ C_g^{(1)} & C_g^{(2)} \end{pmatrix} \begin{pmatrix} \psi^{(1)} \\ \psi^{(2)} \end{pmatrix} = \begin{pmatrix} \phi_0(0) \\ \phi_g(0) \end{pmatrix} \tag{25.17}$$

(We actually saw in Section 13.9 that $\phi_0(0)$ is 1 and $\phi_g(0)$ is 0 because $z = 0$ is the top surface.) We know from Chapters 13 and 14 that the elements of the matrix C are determined by the two-beam conditions that we set up. The matrix C does not depend on z. Now we can use matrix algebra to solve equation 25.17. First rewrite it as

$$C \begin{pmatrix} \psi^{(1)} \\ \psi^{(2)} \end{pmatrix} = \begin{pmatrix} \phi_0(0) \\ \phi_g(0) \end{pmatrix} \tag{25.18}$$

then rewrite equation 25.18 as

$$\begin{pmatrix} \psi^{(1)} \\ \psi^{(2)} \end{pmatrix} = C^{-1} \begin{pmatrix} \phi_0(0) \\ \phi_g(0) \end{pmatrix} \tag{25.19}$$

where C^{-1} is just the inverse matrix. Remember that the order is important in matrix multiplication and that $C^{-1}C = I$, the unit matrix.

Therefore we can rewrite equation 25.14 as

$$\begin{pmatrix} \phi_{\mathbf{0}}(z) \\ \phi_{\mathbf{g}}(z) \end{pmatrix} = C \begin{pmatrix} \exp(2\pi i \gamma^{(1)} z) & 0 \\ 0 & \exp(2\pi i \gamma^{(2)} z) \end{pmatrix} C^{-1} \begin{pmatrix} \phi_{\mathbf{0}}(0) \\ \phi_{\mathbf{g}}(0) \end{pmatrix} \tag{25.20}$$

Finally, we can define a new matrix $P(z)$ as the scattering matrix for a slice of perfect material with thickness z

$$P(z) = C \begin{pmatrix} \exp(2\pi i \gamma^{(1)} z) & 0 \\ 0 & \exp(2\pi i \gamma^{(2)} z) \end{pmatrix} C^{-1} = C\, \Gamma C^{-1} \tag{25.21}$$

The matrix $P(z)$ thus gives us the values of the exit wave amplitudes at the bottom of the slice in terms of the incident values. In other words, the matrix $P(z)$ includes all the information to describe the propagation of the beams through the crystal; $P(z)$ is a *propagator* matrix.

P = C Γ C^{-1} AND VARIES WITH z

Notice that z only enters the 'P equation' through the Γ matrix.

25.4 USING THE SCATTERING MATRIX

Now we illustrate the real strength of the scattering matrix approach by considering the effect of a planar fault lying parallel to the foil surface, as we saw in Figure 25.2. The idea is that we now have two slices of material of thickness t_1 and t_2. We can easily calculate $\phi_{\mathbf{0}}(t_1)$ and $\phi_{\mathbf{g}}(t_1)$ using equation 25.20. These values for $\phi_{\mathbf{0}}$ and $\phi_{\mathbf{g}}$ then become the incident values for slice 2. The effect of the translation $\mathbf{R}$ is to multiply the terms in $C_{\mathbf{g}}$ in the lower slice by a phase factor $\exp(-i\alpha)$ where $\alpha = 2\pi \mathbf{g} \cdot \mathbf{R}$ as usual. The matrix C for slice 2 is then written as

$$C_2 = \begin{pmatrix} C_{\mathbf{0}}^{(1)} & C_{\mathbf{0}}^{(2)} \\ C_{\mathbf{g}}^{(1)} \exp(i\alpha) & C_{\mathbf{g}}^{(2)} \exp(i\alpha) \end{pmatrix} \tag{25.22}$$

We can write down the expression for $\phi_{\mathbf{0}}(t)$ and $\phi_{\mathbf{g}}(t)$ as

$$\begin{pmatrix} \phi_{\mathbf{0}}(t) \\ \phi_{\mathbf{g}}(t) \end{pmatrix} = C_2 \Gamma(t_2) C_2^{-1} C_1 \Gamma(t_1) C_1^{-1} \begin{pmatrix} \phi_{\mathbf{0}}(0) \\ \phi_{\mathbf{g}}(0) \end{pmatrix} \tag{25.23}$$

Here the subscripts on C_1 and C_2 just identify the slices. Normally, this equation goes straight into the computer, which handles matrices very easily. However, we'll go back and consider a few special points

- Look at equation 25.22 and set $\mathbf{R} = 0$ so that $C_2 = C_1$. You can see that $P(t) = P(t_1)P(t_2)$. Clearly we could cut the perfect-crystal specimen into many slices and $P(t)$ would always be the product of the scattering matrices for each slice. (We could call this a multislice approach to scattering from a crystal but we don't to avoid confusion with HRTEM simulation.)
- How do we prove equation 25.22? From equation 14.12 we know that a Bloch wave can be written as

$$b(\mathbf{k}) = \sum_{\mathbf{g}} C_{\mathbf{g}}(\mathbf{k}) \exp(2\pi i(\mathbf{k} + \mathbf{g}) \cdot \mathbf{r}) \tag{25.24}$$

- If the lower crystal is displaced by a vector $\mathbf{R}$ then we replace $\mathbf{r}$ by $\mathbf{r} - \mathbf{R}$ (notice the sign). (We have just used a 'hidden' column approximation.) Equation 25.24 is then written as

$$b(\mathbf{k}) = \sum_{\mathbf{g}} C_{\mathbf{g}}(\mathbf{k}) \exp(2\pi i(\mathbf{k} + \mathbf{g}) \cdot (\mathbf{r} - \mathbf{R})) \tag{25.25}$$

$$b(\mathbf{k}) = e^{-2\pi i \mathbf{k} \cdot \mathbf{R}} \sum_{\mathbf{g}} C_{\mathbf{g}}(\mathbf{k}) e^{(-2\pi i \mathbf{g} \cdot \mathbf{r})} e^{2\pi i(\mathbf{k}+\mathbf{g}) \cdot \mathbf{r}} \tag{25.26}$$

$C_{\mathbf{0}}$ is not affected by $\mathbf{R}$ since than $2\pi \mathbf{0} \cdot \mathbf{R} = 0$, but $C_{\mathbf{g}}$ is multiplied by $e^{-i\alpha}$.
- If you choose the coordinates appropriately then C is a unitary matrix. In this case, you can find C^{-1} just by reflecting across the diagonal and taking the complex conjugate of each term. This *trick* will allow you to express equation 25.23 explicitly, as given by Hirsch et al. (omitting a phase factor).

$$\begin{aligned} \phi_{\mathbf{0}}(t) = &[\cos(\pi \Delta k t) - i \cos(\beta) \sin(\pi \Delta k t)] \\ &+ \frac{1}{2}\left(e^{i\alpha} - 1\right) \sin^2 \beta \cos(\pi \Delta k t) \\ &- \frac{1}{2}\left(e^{i\alpha} - 1\right) \sin^2 \beta \cos(\pi \Delta k t') \end{aligned} \tag{25.27}$$

$$\begin{aligned} \phi_{\mathbf{g}}(t) = &\, i \sin(\beta) \sin(\pi \Delta k t) \\ &+ \frac{1}{2} \sin \beta \left(1 - e^{(-i\alpha)}\right) [\cos \beta \cos(\pi \Delta k t) - i \sin(\pi \Delta k t)] \\ &- \frac{1}{2} \sin \beta \left(1 - e^{(-i\alpha)}\right) [\cos \beta \cos(\pi \Delta k t') - i \sin(\pi \Delta k t')] \end{aligned} \tag{25.28}$$

In equations 25.27 and 25.28, t' is the distance of the fault below the center of the slice, i.e., we define $t' = t_1 - t/2$ where t_1 lies between 0 and t. (It's a good, but tedious, exercise to derive these equations for yourself.) The right-hand side of equations 25.27 and 25.28 each contains three terms.

- The first term is just what we found in Chapter 13 where the phase factor $\alpha = 0$, i.e., it's just like the perfect crystal.
- The second term is independent of the position of the planar fault because it doesn't depend on t'.

- The third term depends on t' such that both ϕ_0 and ϕ_g change with a periodicity in t' given by Δk^{-1}. So these amplitudes show the same dependence on ξ_g^{eff}. They will both show thickness variations.

THE GEOMETRY
You should keep in mind that we derived these equations for a planar defect lying parallel to the parallel surfaces of our specimen and normal to the beam.

We can now take these ideas and apply them to planar defects which are inclined to the surface, by calculating the contrast for all values of t' between 0 and t. The important points to remember are

- The model used in the calculation was a flat interface parallel to the surface of a plate-like specimen. You'll see fault fringes when t' varies across the fault but you don't usually have to consider the fact that either the surface or the fault may be inclined to the beam.
- The concept of the scattering matrix allows you to identify very clearly the effect of the defect on ϕ_0 and ϕ_g.

25.5 STACKING FAULTS IN FCC MATERIALS

We'll begin our discussion of actual examples with the SF in fcc materials. Before we discuss the details of contrast from SFs in fcc materials, we'll summarize the important results which hold for all planar defects

- The appearance of the image depends on the specimen thickness.
- Pairs of BF/DF SF images are not generally complementary even though we are using a two-beam approximation. Compare to the complementary behavior of the thickness fringes discussed in Chapter 24.
- Planar defects always really have a thickness. We'll illustrate this concept using overlapping faults in fcc materials (see also Section 26.6).

NOT ALL MATERIALS ARE FCC
Do not assume all faults are the same as in fcc materials!

25.5.A Why fcc Materials?

There are several reasons for emphasizing the analysis of stacking faults in fcc crystals

- Many important materials are fcc, including the metals Cu, Ag, Au, and austenitic stainless steel, and the semiconductors Si, Ge, and GaAs.
- Most of the analysis of SFs derives from the study of fcc materials.
- The translations are well known and directly related to the lattice parameter: **R** is either $1/6<\bar{1}\bar{1}2>$ or $1/3<111>$. Notice that these definitions differ by the lattice vector, $1/2<110>$. (Actually there may be small deviations from these ideal values but we'll ignore them for now.)

We want to learn how to extend this analysis to other fault vectors and avoid making unfounded assumptions when we do extend it. The geometry often encountered when studying defects in fcc materials is shown in Figure 25.3.

You should note that $(11\bar{1})$ is one of three possible planes for an inclined SF. In this case, the translation at the stacking fault will be $\mathbf{R} = \pm 1/3[11\bar{1}]$; the phase factor, α, is $2\pi\,\mathbf{g}.\mathbf{R}$. If we form an image with the $\mathbf{g} = (2\bar{2}0)$ reflection strongly excited then $\mathbf{g}.\mathbf{R} = 0$ and the fault is out of contrast in both BF and DF. If instead we use the reflection $\mathbf{g} = (02\bar{2})$ then $\mathbf{g}.\mathbf{R} = 4/3$ or $-4/3$ and $\alpha = 8\pi/3 = 2\pi/3 = 120°$ or $-8\pi/3 = -2\pi/3 = -120°$ (modulo 2π in each case). Notice that if the stacking fault lies parallel to the surface of this (111)-oriented specimen, you must tilt the specimen to see *any* contrast from the SF, i.e., $\mathbf{g}.\mathbf{R} = 0$ for all values of **g** lying in the fault plane.

INVISIBILITY CRITERION
When $\mathbf{g}.\mathbf{R} = 0$ the defect is 'out of contrast'; it's invisible.

Figure 25.4A and B shows two typical BF/DF pairs of $\pm\mathbf{g}$ strong-beam images from the same SF. In the BF images, the outer fringes are the same on both sides of the fault, both gray or both white while in the DF images one outer fringe is white but the other is gray. The questions which arise are

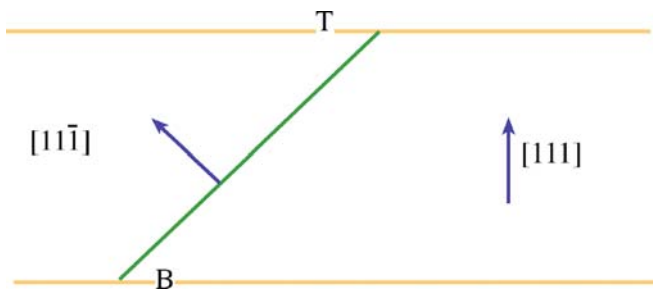

FIGURE 25.3. A stacking fault in a parallel-sided fcc specimen. The normal to the specimen is [111] and the normal to the SF is [11$\bar{1}$]. T and B indicate the top and bottom of the foil.

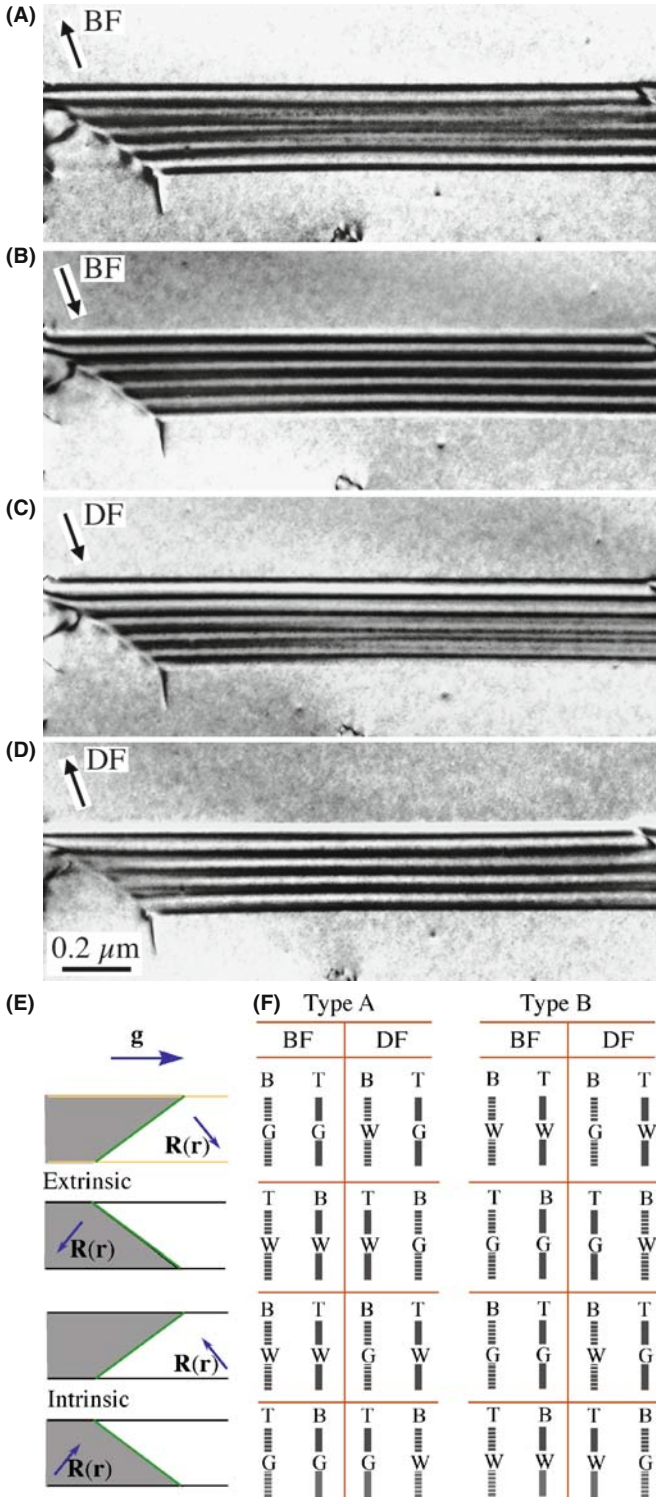

FIGURE 25.4. (A–D) Four strong-beam images of an SF recorded using $\pm\mathbf{g}$ BF and $\pm\mathbf{g}$ DF. The beam was nearly normal to the surfaces; the SF-fringe intensity is similar at the top surface but complementary at the bottom surface. The rules are summarized in (E) and (F) where G and W indicate that the first fringe is gray or white; (T, B) indicates top/bottom.

- What determines whether a fringe will be gray or white?
- Why are the two images not complementary?

Note that in the summary schematic shown in Figure 25.4E, 200, 222, and 440 are type A reflections while 111, 220, and 400 are type B reflections. Also we'll call the first fringe gray (G), not black (i.e., B), to reduce confusion!

25.5.B Some Rules

There are some experimental rules

- Be very careful when you record such a pair of images: record the DP for each image. Be sure to note which of the two bright spots corresponds to the direct beam.
- Use the same strong *hkl* reflection for BF and DF imaging. Therefore, to form the CDF image using a strong *hkl* reflection, you must first tilt the specimen so that $\bar{h}\bar{k}\bar{l}$ is strong and then use the beam tilts to move *hkl* onto the optic axis where it will become strong (see Section 22.5). This is confusing, so we recommend that you sacrifice a little image resolution and compare the BF image with a displaced-aperture DF (DADF) image, rather than a CDF image.

This is exactly the opposite of the approach used by Edington, who advocates tilting in $\bar{h}\bar{k}\bar{l}$ for the DF image, which reverses the DF contrast in Figure 25.4E and F. Our approach ensures that diffraction from the same *hkl* planes causes the contrast in both DF and CDF images but DADF beats both! (TEMs were not as good in 1975 as they are now.)

Then there are some rules for interpreting the contrast

- In the image, as seen on the screen or on a print, the fringe corresponding to the top surface (T) is white in BF if $\mathbf{g}\cdot\mathbf{R}$ is > 0 and black if $\mathbf{g}\cdot\mathbf{R} < 0$.
- Using the same strong *hkl* reflection for BF and DF imaging, the fringe from the bottom (B) of the fault will be complementary whereas the fringe from the top (T) will be the same in both the BF and DF images.
- The central fringes fade away as the thickness increases. If this seems anomalous, the explanation is in Section 25.10.
- The reason it is important to know the sign of $\mathbf{g}$ is that you will use this information to determine the sign of $\mathbf{R}$.
- For the geometry shown in Figure 25.3, if the origin of the $\mathbf{g}$ vector is placed at the center of the SF in the DF image, the vector $\mathbf{g}$ points away from the bright outer fringe if the fault is extrinsic and toward it if it is intrinsic (200, 222, and 440 reflections); if the reflection is a 400, 111, or 220 the reverse is the case.

- Don't forget that, as we said at the start of Chapter 22, any contrast must be >~5–10% to be visible to the eye, so we traditionally say an intensity change due to $\mathbf{g}.\mathbf{R}$ effects is only detectable if $\mathbf{g}.\mathbf{R} > 0.02$; of course, now you can digitally record the TEM image or digitize your analog version and then process this so the limit could be lower. With experience, you'll find there is an optimum thickness to view defect contrast, before absorption effects make it difficult. You must also carefully select **s** so that the background intensity in the matrix around the defect is gray and this maximizes visibility of lighter and darker fringes.

DISPLACE THE APERTURE

To avoid the possibility of confusion about which reflection to use for the DF image, just displace the aperture to the strong *hkl* reflection in every case. In a modern IVEM, there is almost no loss of resolution between DADF and CDF. DADF is always preferred but CDF is used to give much better images.

As we said, these complex rules are summarized in Figure 25.4C and D. Although they are very useful, in practice you should remember that they were derived for a very special combination of **R** and **g** in fcc materials. Some important examples of $\mathbf{g}.\mathbf{R}$ are given in Table 25.2. As we'll describe in Section 25.11, if this is your research, you should use a computer program to check the contrast.

INVISIBILITY

Just because you can't see a defect doesn't mean it isn't there or that $\mathbf{g}.\mathbf{R} = 0$.

25.5.C Intensity Calculations

Now let's consider intensity calculations using the column approximation, which we briefly discussed in Section 13.11. If the fault cuts the column at a depth t_1 we can deduce from equations 25.22 and 25.23 that

$$\phi_{\mathbf{g}} = \frac{i\pi}{\xi_{\mathbf{g}}}\left\{\int_0^{t_1} e^{-2\pi i s z}dz + e^{-i\alpha}\int_{t_1}^{t} e^{-2\pi i s z}dz\right\} \qquad (25.29)$$

TABLE 25.2. Values of $\mathbf{g}.\mathbf{R}$ for Some Common R Plus g Combinations

	R	g	$\alpha = 2\pi\,\mathbf{g}.\mathbf{R}$ (mod 2π)
SF in fcc	$\frac{1}{3}[111]$	(111), (220), (113)	$2\pi/3$
SF in fcc	$\frac{1}{3}[111]$	(113)	$4\pi/3$
Translation at APB in Fe_3Al	$\frac{1}{2}[110]$	(100)	π
Small **R**, e.g., NiO	Any	**g** or **s** or $\xi_{\mathbf{g}}$ differ slightly	δ

which gives

$$\phi_{\mathbf{g}} = \frac{i\pi}{s\xi_{\mathbf{g}}} e^{-2\pi i s t_1}\left\{\sin(\pi s t_1) + e^{-i\alpha}\sin(\pi s(t-t_1))\right\} \qquad (25.30)$$

We rearrange equation 25.30 to give an expression for the intensity, $I_{\mathbf{g}}$ $(=\phi_{\mathbf{g}}\cdot\phi_{\mathbf{g}}^*)$. This rearrangement involves a little manipulation.

$$I_{\mathbf{g}} = \frac{1}{(s\xi_{\mathbf{g}})^2}\left\{\sin^2\left(\pi s t_1 + \frac{\alpha}{2}\right) + \sin^2\left(\frac{\alpha}{2}\right) - \sin\left(\frac{\alpha}{2}\right)\sin\left(\pi s t + \frac{\alpha}{2}\right)\cos(2\pi s t')\right\} \qquad (25.31)$$

where $t' = t_1 - t/2$ as before. So the contrast depends on both the thickness and the depth. Note that $t/2$ is the center of the foil. Since α is fixed for a particular defect, let's fix t. Then equation 25.31 becomes

$$I_{\mathbf{g}} \propto \frac{1}{s^2}\{A - B\cos(2\pi s t')\} \qquad (25.32)$$

Now we have cosine depth fringes or defect thickness fringes, just as we did for the perfect crystal

- The thickness periodicity depends on s^{-1}.
- The intensity varies as s^{-2}.

We could have derived this equation from equation 25.28 with more work. However, the value of the scattering matrix approach is that we don't derive the analytical expression but just run the computer program.

In Chapter 27, we will discuss this SF contrast in terms of phasor diagrams which give a graphical way to represent these equations.

25.5.D Overlapping Faults

It is interesting to extend this analysis to the case of overlapping faults. Taking the analytical approach, we can extend equation 25.29 to the case of two overlapping faults, the first at depth t_1 and the second at depth t_2.

$$\phi_{\mathbf{g}} = \frac{i\pi}{\xi_{\mathbf{g}}}\left\{\int_0^{t_1} e^{-2\pi i s z}dz + e^{-i\alpha}\int_{t_1}^{t_1+t_2} e^{-2\pi i s z}dz + e^{-i(\alpha_1+\alpha_2)}\int_{t_1+t_2}^{t} e^{-2\pi i s z}dz\right\} \qquad (25.33)$$

An experimental illustration of a somewhat more complex situation, involving several overlapping SFs, is shown in Figure 25.5

- It sometimes appears that there is no contrast, even when we know that there are overlapping SFs. This can happen if, e.g., three SFs overlap on adjacent (or nearly adjacent) planes; then the effective R can

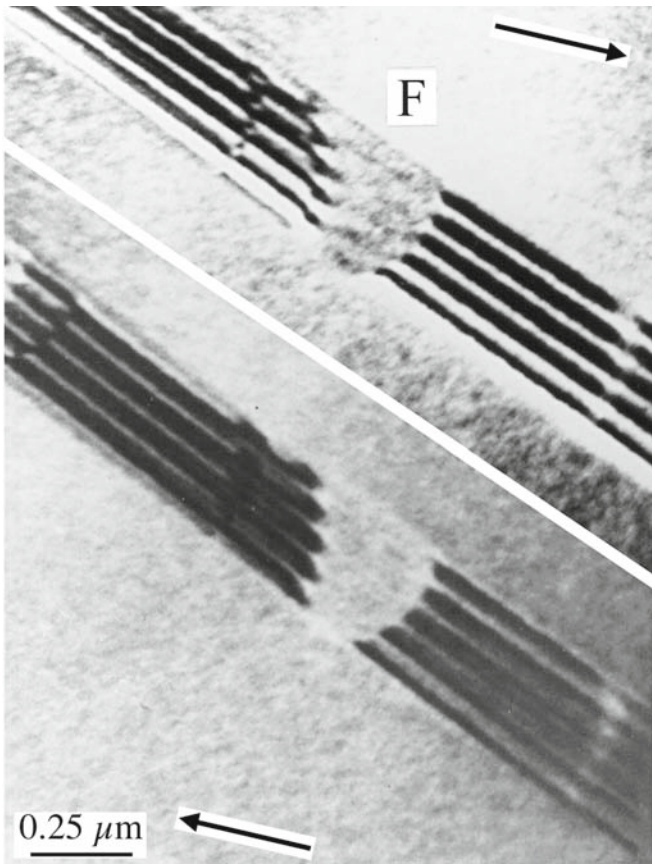

FIGURE 25.5. Two BF images of overlapping SFs in fcc steel with the direction **g** indicated. The faults are very close together. When three faults overlap at F the effective value of **R** is 0 so the contrast disappears.

be $= 3 \times \frac{1}{3}[11\bar{1}]$, which is a perfect lattice vector and can therefore appear to give $2\pi\mathbf{g}\cdot\mathbf{R} = 0$.

We will return to this topic in Section 27.8, where we'll show that some planar defects, such as the extrinsic SF in Si, or the dissociated {112} twin boundary in some fcc metals, really have a significant thickness. We can then analyze the contrast from such interfaces using the overlapping-fault model.

25.6 OTHER TRANSLATIONS: π AND δ FRINGES

We discussed the $L1_0$ structure of NiAl in Section 16.5. This intermetallic is an example of a large group of materials which can contain a different type of RB. If the Ni atoms sit at the corners of the cell in one crystal region but the Al atoms sit at the corners in another part of the crystal, then the two crystal regions are related by a translation of $\frac{1}{2}[111]$. The two crystals would otherwise still be perfectly aligned but are separated by this RB, which we call an APB (but which could be called an SF or an IDB).

Similarly in the $L1_2$ structure of the intermetallic Ni_3Al, we could have the Al atoms on the corners of the unit cell in one part of the crystal and displaced by $\mathbf{R} = \frac{1}{2}[110]$ in the adjacent region. (We can actually form six non-equivalent APBs in this structure and these are *not* IDBs.) The crystal structure looks like fcc but the Al atoms are at the corners of the unit cell (forming the simple-cubic superlattice) with the Ni at the face-centered positions. The easy way to appreciate this RB is to think what would happen if the alloy were completely disordered: there would be no planar defect. This RB can be imaged using the (100) reflection. Notice again that for a disordered structure, the {100} reflections would be absent if the alloy were disordered; the {100} planes are said to give rise to superlattice reflections; these reflections would be forbidden if the material were disordered. For this case we can readily show that the phase factor $\alpha = \pi$, so the fringes we see are called π fringes. The structure of this interface is shown schematically in Figure 25.6. These π fringes can give symmetric fringes in DF and BF and complementary DF/DF pairs.

SUPERLATTICES

We usually use the term *superlattice* in the sense that it is the *real* lattice, because we have ordering of the components. If the same material was disordered (but with the atoms on the same sites), the lattice parameters, in real space, would be smaller.

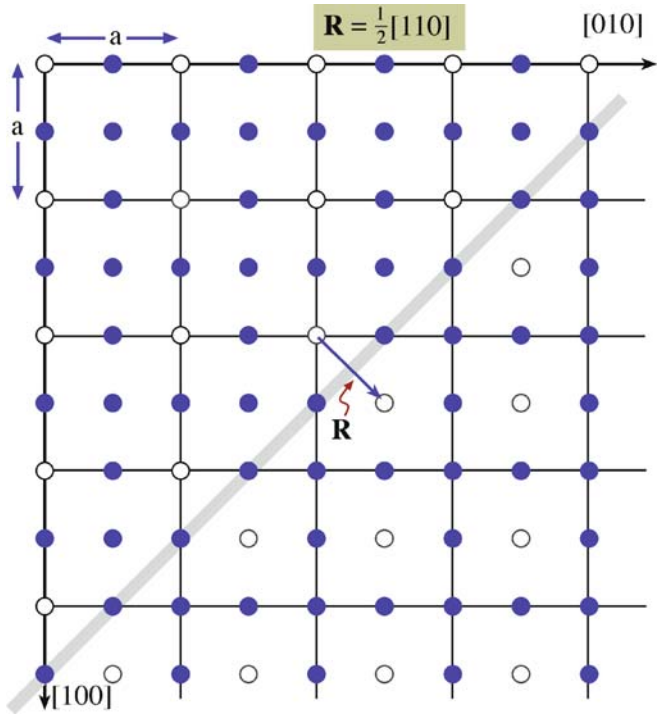

FIGURE 25.6. Schematic of an interface in the intermetallic Ni_3Al showing how the two structures link coherently but are displaced by the vector **R**. The phase factor at such an interface is π and the fringes seen in the image are called π fringes.

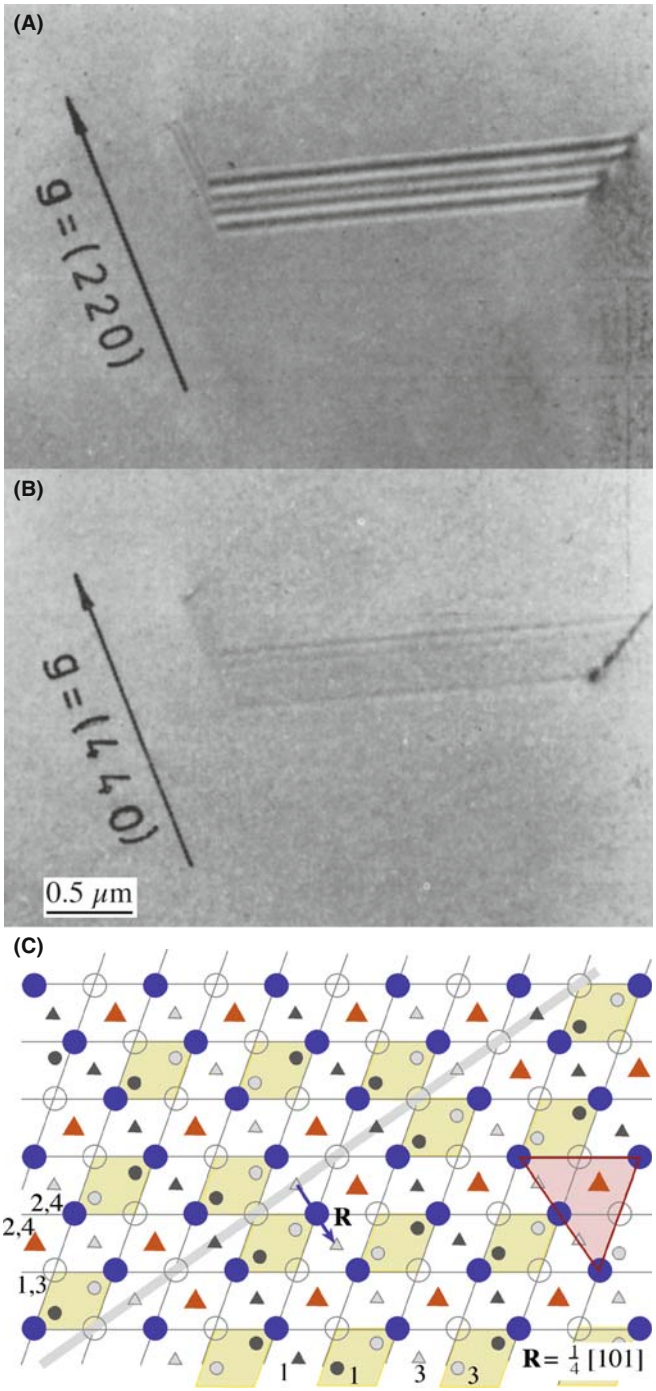

FIGURE 25.7. (A, B) Pair of BF images and (C) schematic of an SF in spinel; this interface is also known as an APB since the SF translation vector is a perfect (sub)lattice vector in the underlying fcc oxygen sublattice as shown in (C). Large circles are O anions at different heights (1, 3) and (2, 4); the small circles and triangles are cations at different heights (1–4 as indicated). (D) APBs can overlap just as SFs can as shown by these faceted APBs in TiO_2. Many of the facets give quite similar contrast but those near the center are strikingly different because of overlap. The schematic (E) shows a series of APBs, each of which is formed by a translation, $\mathbf{R} = {}^1/_2[011]$ which has little effect of the oxygen sublattice (open circles).

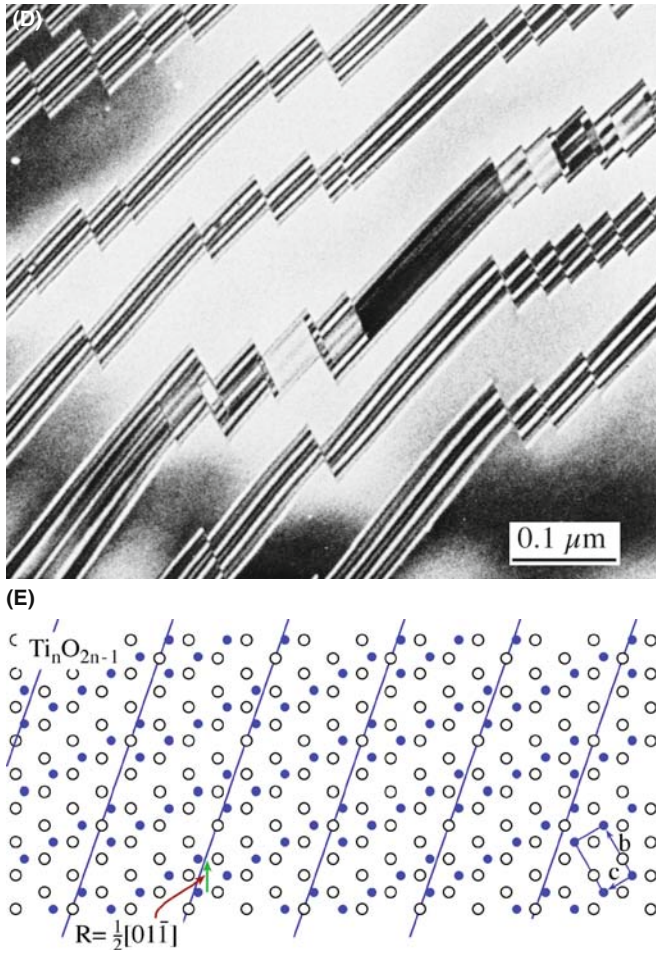

FIGURE 25.7. (Continued).

Similar RBs are very common in oxides because the unit cell is often quite large, giving more opportunities to form such interfaces. The interface shown in Figure 25.7A and B has been called both an SF and an APB in spinel. These interfaces can show all the features we discussed in Section 25.5 for SFs in fcc materials, and those we've just discussed depend on which reflection you use. You can again see a change in contrast in Figure 25.7D when APBs in TiO_2 overlap as shown schematically in Figure 25.7E (Amelinckx and Van Landuyt 1978). In Figure 25.7A and B, if you image the fault using the 220 reflection $2\pi\mathbf{g}\cdot\mathbf{R} = \pi$ and so you'll see SF fringes. If, however, you image using 440, $2\pi\mathbf{g}\cdot\mathbf{R} = 2\pi$, so you'll only see residual contrast (because **R** is not exactly $\frac{1}{4}[101]$.

The APB shown in Figure 25.8A is different yet again. This planar defect in GaAs is also known as an IDB (Section 25.1). The fringes you see are caused by a translation, but **R** is not related in a simple way to the structure of the crystal or to the inversion symmetry. Rasmussen et al. showed that the translation is present because there is a small relaxation of the Ga–Ga and As–As bonds at this {110} interface. The value of **R** was determined to be 0.19 Å with a statistical uncertainty of ±0.03 Å, so it's a translation that's almost parallel to the

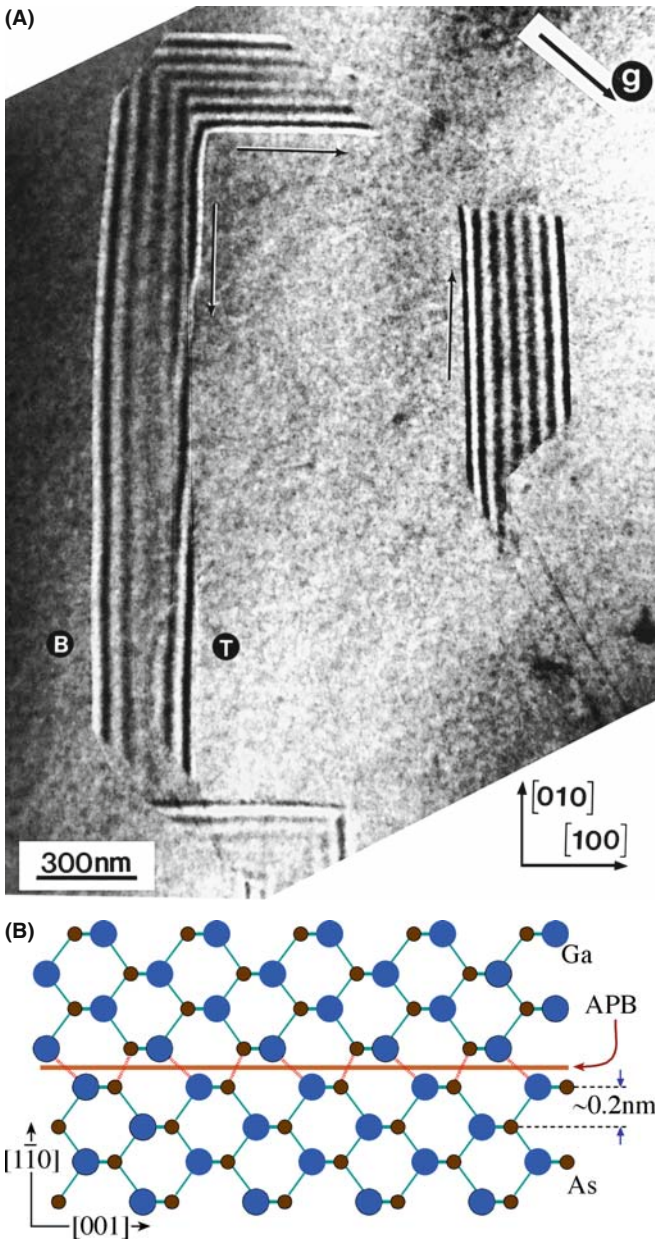

FIGURE 25.8. (A) A faceted APB (or IDB) in GaAs with (B) a schematic of the (110) facet. The translation is caused by the difference in length of the Ga–Ga and As–As bonds and is much smaller than a lattice vector in the GaAs lattice.

interface, as shown schematically in Figure 25.8B. These fringes are then known as δ fringes (because there is only a small translation and α is not related in a simple way to 2π). The use of image-simulation programs, which are necessary to determine **R** (remember that the wavelength of the 200-kV electrons used for the measurement is itself 0.025 Å or 2.5 pm), is discussed in Section 25.13.

25.7 PHASE BOUNDARIES

We'll list a few special phase boundaries in Table 25.3.

TABLE 25.3 Examples of Special Phase Boundaries

Boundary	Example of material	Features
Ferromagnetic domain boundaries	NiO	
Ferroelectric and piezoelectric boundaries	$BaTiO_3$	Small tetragonal distortion
Composition boundary	GaAs/AlGaAs	$\xi_{\mathbf{g}}$ is different on two sides of boundary, even for perfect lattice matching
Structure boundaries	α-SiC/β-SiC hcp-Co/fcc-Co	
Composition/structure	NB/Al_2O_3 Al/Cu α-Fe/Fe_3C	

An example of a PB is shown in Figure 25.9. In NiO, which is ferromagnetic, some of the planes rotate slightly when the structure changes from cubic symmetry below the Curie temperature. Now we can also define the cubic structure as rhombohedral with $\alpha = 60^\circ$ in the rhombohedron. Below the Curie temperature, the rhombohedral angle is distorted by only 4.2′ (yes, minutes of arc) from the true 60°. Therefore, most **g**-vectors will rotate through a very small angle and hence produce a change in the value of **s**. However, as you can see in Figure 25.9, this small rotation can readily be detected by the change in contrast and the faint fringes at the phase boundary.

We can have overlapping PBs, so, the warning is the same: be very wary and use tilting experiments while you are at the TEM.

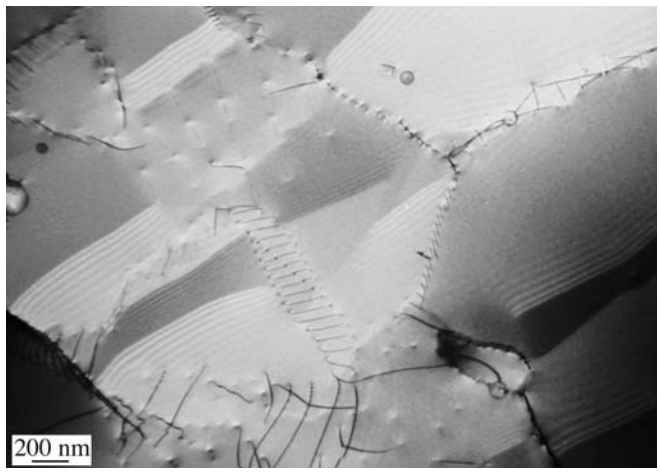

FIGURE 25.9. The ferroelectric material NiO undergoes a structural change from cubic to distorted rhombohedral at the Curie temperature. Although the distortion in the rhombohedral structure is very small, it does cause a detectable rotation of the lattice planes that results in the δ fringes in the image.

25.8 ROTATION BOUNDARIES

What can we learn about rotation boundaries when the rotation angle is greater than about 0.1°? Unfortunately, the answer is "not a lot," unless we have defects which accommodate the rotation. Then we are into the subject of diffraction contrast of line defects in interfaces. However, with care you may be able to excite **g** in one grain or in both by tilting the specimen. The difficulty, of course, is that $\mathbf{s_g}$ is likely to be different in each material. Complications will also arise if other defects are present, since you may or may not see those defects. Examples of such inclined, rotation interfaces are shown schematically in Figure 25.10A and experimentally in Figure 25.10B and C.

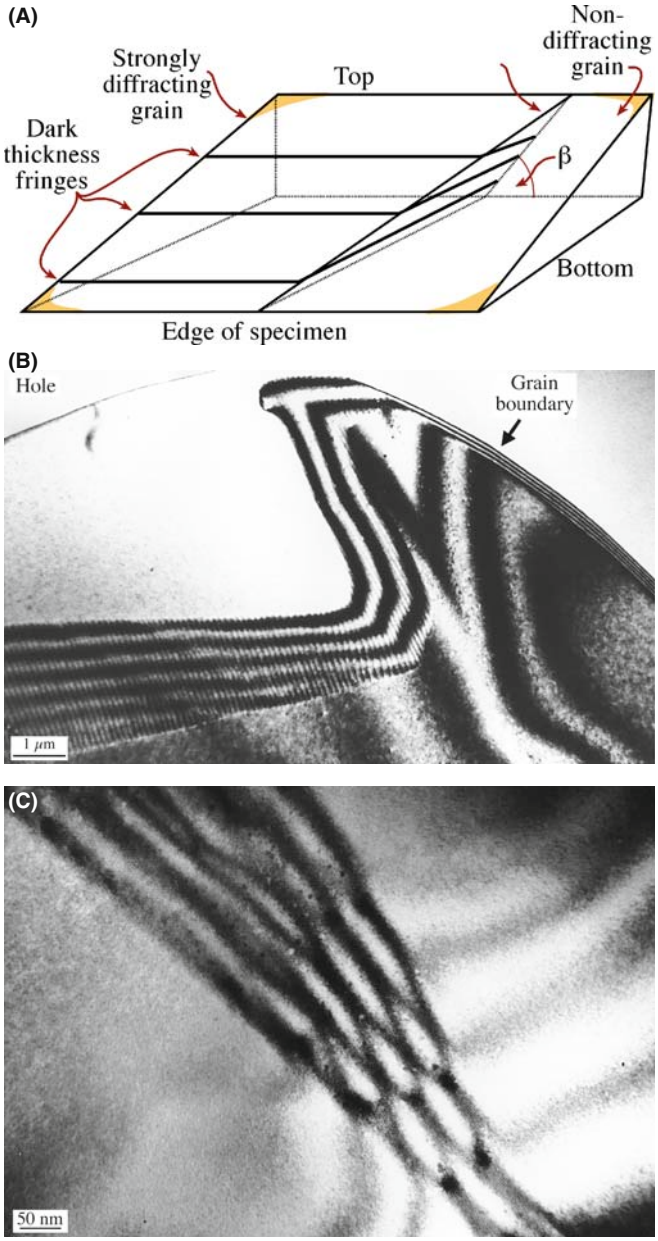

FIGURE 25.10. (A) If the adjoining grains are rotated so that they do not share a common reflection, images can be formed where only one of the grains diffracts. As shown in (B), the thickness fringes associated with the wedge merge into the thickness fringes associated with the inclined interface. (C) If the foil is tilted so that the same (though not coincident) reflection is excited in both grains, the number of fringes in the interface increases with each incremental increase in the wedge thickness.

25.9 DIFFRACTION PATTERNS AND DISPERSION SURFACES

You read in Chapter 17, that what you see in an image must be related to what happens in the DP which in turn is determined by how the Ewald sphere intersects the reciprocal lattice. Figure 17.5 showed that a planar defect which is inclined to the surface of a parallel-sided specimen will give rise to relrods. Therefore, a planar defect that is inclined to the surface of a parallel-sided specimen will produce at least two spots in the DP. Since most specimens are wedges (see Figure 17.4), and the planar defect will, in general, be inclined to both surfaces, the relrod geometry is actually even more complex. Figure 25.11 shows lines normal to each interface and their associated relrods. You can appreciate that when the Ewald sphere cuts these relrods, several spots may appear in the DP. Now we need to relate these relrods to the fringes we see in the image. This model would predict that we would not produce fringes when $\mathbf{s} = 0$, so we should modify what we did in Figure 17.15. The periodicity of the fringes in the image is inversely related to the distances (M_1N and M_2N) between the spots in the DP.

FRINGE SPACING

At $\mathbf{s} = 0$, the thickness fringe spacing is determined by $\Delta k = \xi_{\mathbf{g}}^{-1}$ and the wedge angle: the spacing of the fringes is proportional to $\xi_{\mathbf{g}}$.

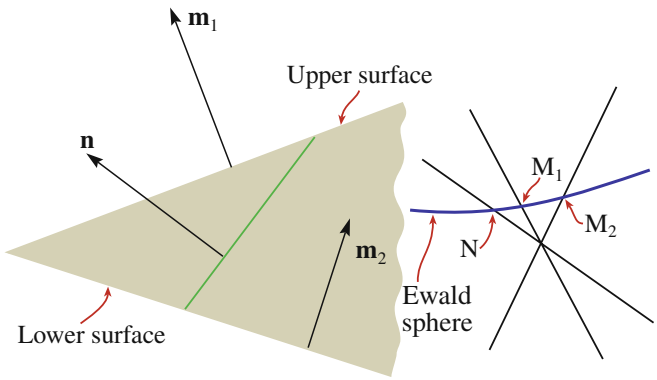

FIGURE 25.11. In a wedge specimen, the planar defect will, in general, be inclined to both surfaces and the relrod geometry is complex. The fringe spacing in the image is related to the reciprocal of the distances M_1N and M_2N.

When a planar defect is present in the specimen, the two branches of the dispersion surface are not only coupled along a tie-line normal to the surface of the specimen but also along the normal to the planar defect. However, when $\mathbf{s} = 0$, the thickness periodicity in the image corresponds to the extinction distance. When we relate this to the region G in the reciprocal lattice, the two relrods (which result from a kinematical construction) must actually separate to give the two hyperbolas shown in Figure 25.12 which is why we drew Figures 17.15 and 23.6 as we did.

FRINGES IMPLY SPOTS
If you see fringes in the image, spots will be present in the DP.

The spots in the DP are associated with points M and N in Figures 25.11 and 25.12.

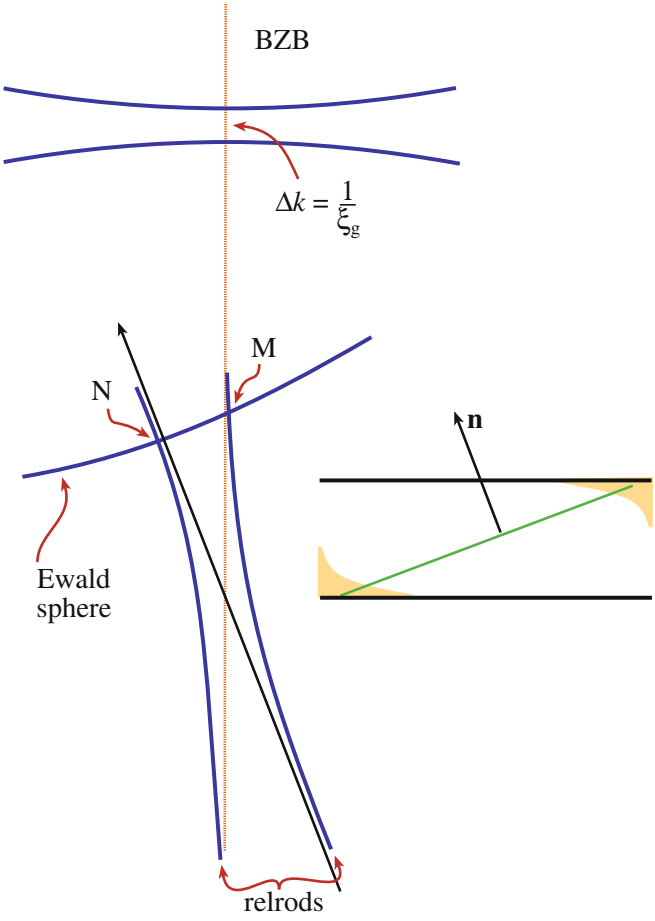

FIGURE 25.12. The dispersion-surface construction for an inclined planar defect in a parallel-sided specimen. (Compare Figures 17.15 and 24.6.) For simplicity, we show the hyperbolas due to the defect alone, not the extra effects that would arise in a wedge specimen.

25.10 BLOCH WAVES AND BF/DF IMAGE PAIRS

In Chapter 14 we saw that, in a crystal, the electron must propagate as Bloch waves, and yet we have not mentioned Bloch waves in our discussion of thickness and bending so far. Most of the analysis of this topic is beyond the scope of this text, but it is important to understand the basic ideas, particularly since they will also apply to scattering from defects in the crystals. Remember that ξ_g is a direct consequence of having two Bloch waves. The important message here is: don't let the words overawe you.

The idea is quite simple. Since we have two Bragg beams excited, then we must have two Bloch waves in the crystal. The propagation vectors of these two waves are $\mathbf{k}_1$ and $\mathbf{k}_2$ with the difference $|\Delta\mathbf{k}|$ being related to s_{eff} (and $\gamma_1 - \gamma_2$ in Section 13.10). We see a thickness dependence in the image because the two waves are interfering. The only two waves which are really present in the crystal are the two Bloch waves. It's the beating of these two waves which gives rise to thickness effects.

In the two-beam case, the Bloch waves, 1 and 2, are channeled along and between the atom columns (see Figure 14.2). A fault may change the channeled wave into the non-channeled one, as you can see in Figure 25.13. So, the effect of the planar defect is to couple the

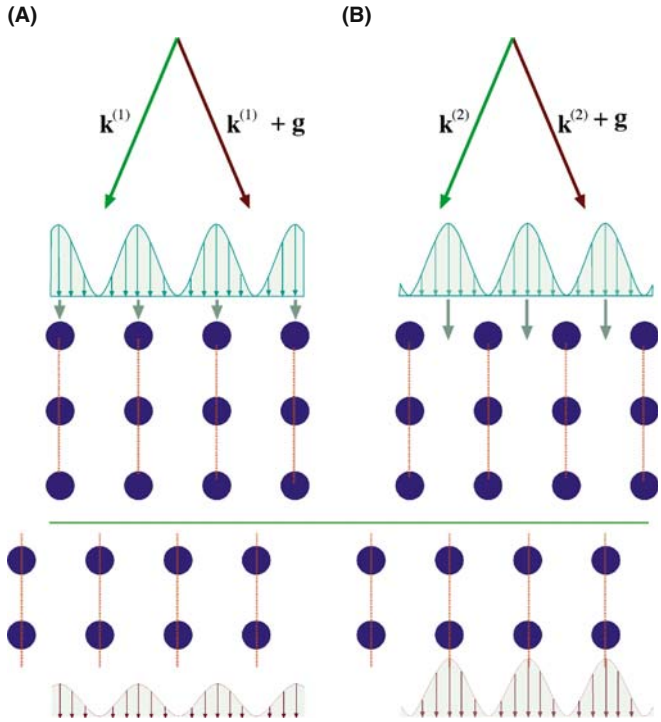

FIGURE 25.13. Bloch waves 1 and 2 are channeled (A) along and (B) between the atom columns, respectively, until they meet the fault. There the atomic columns are translated so that the channeled Bloch wave may become the non-channeled one and vice versa.

Bloch waves; in other words, the defect links (or connects or ties) the different branches of the dispersion surface (along the tie line). The non-complementary contrast at SFs in fcc metals is directly explained by this coupling.

As soon as the beam enters the specimen we excite Bloch waves 1 and 2. Therefore, in Figure 25.14A, the two Bloch waves 1 and 2 are shown everywhere at the top surface of the foil. The planar defect links points D_1 and D_2 on the two branches of the dispersion surface, as shown in Figure 25.14B, along the tie line, D_1D_2' and $D_1'D_2$. We'll analyze the three situations shown in Figure 25.14A, which correspond to the planar defect being close to the top, the middle, and the bottom of the specimen. The key feature is that, as we saw in Section 14.6, Bloch wave 1, which has the larger **k**-vector, will be preferentially absorbed. It is actually totally absorbed in thicker specimens.

- When the planar defect is close to the top surface (as occurs near T in Figure 25.14A), waves 1 and 2 are both coupled (or scattered) to the other branch of the dispersion surface so we form four Bloch waves (but with only two **k**-vectors). Both Bloch waves which are associated with the upper branch of the dispersion surface (wave vector $\mathbf{k}_1$) are preferentially absorbed, but the waves D_2 and D_2' both reach the lower surface. There, they interfere to give the thickness fringes even though they are both associated with the lower branch of the dispersion surface; D_2' retains a 'memory' of D_1.
- When the fault is close to the middle of the specimen in Figure 25.14A, the branch-1 Bloch wave is absorbed before it reaches the planar defect but a new Bloch wave D_1' is formed at the defect. However, while traversing the other half of the foil, this wave is also absorbed so that only wave D_2 reaches the lower surface. Thus the electrons can propagate through the specimen (we can see through it) but there are no thickness fringes because only one Bloch wave survives. However, we can still image defects in these thicker areas, as you'll see if you look back at Figure 23.10.
- At the lower surface, B in Figure 25.14A, only wave D_1 survives to reach the planar defect but it now produces a new wave D_1' which can reach the lower surface, recombine with Bloch wave D_2, and produce thickness fringes. The resulting contrast is summarized in Figure 25.14C.

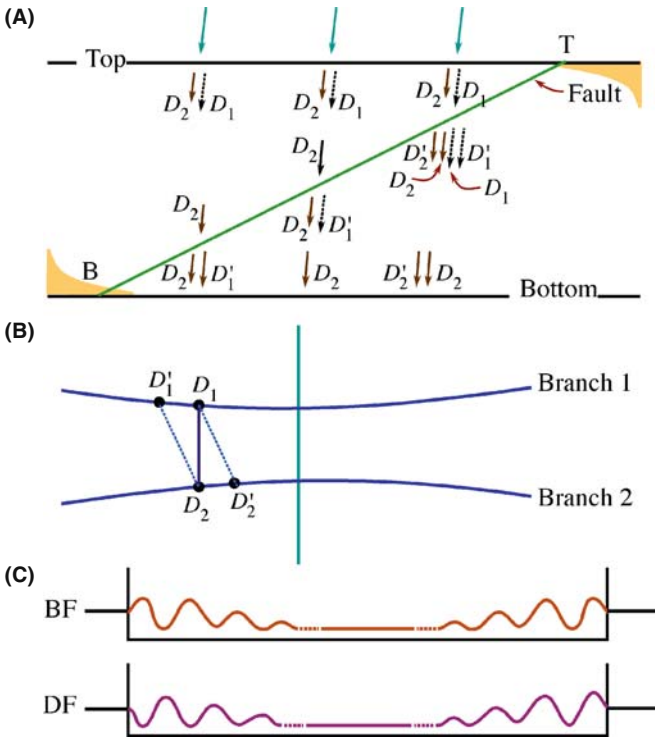

FIGURE 25.14. The absorption of the branch-1 Bloch wave near the top surface, T, of the specimen and its re-creation when the planar defect is near the bottom, B, determines the contrast we see. (A) shows which Bloch waves are present at the different depths in the specimen, (B) shows how the Bloch waves are coupled along tie lines joining the two branches of the dispersion surface, and (C) shows the resulting contrast profiles.

Bloch-wave absorption is a critical factor in explaining the appearance of contrast from planar defects. The part of this argument which is not intuitive is the fact that D_2' retains a memory of D_1; this memory allows it to interfere with D_2 to produce the thickness fringes near the top of the specimen, even though no Bloch wave from branch 1 reaches the bottom of the specimen. We'll refer you to the article by Hashimoto et al. for further discussion on this topic.

25.11 COMPUTER MODELING

From the discussion in Sections 25.5 and 25.6, you will realize that α and π fringes are usually understandable as long as you know what the defect is and as long as it's not actually a set of overlapping defects. The contrast from δ fringes is much more complex and combinations of α, π, and δ fringes are difficult! The situation will become even more complicated if you want to understand the contrast occurring when other defects interact with these planar faults.

A computer program is then really the only way to analyze the contrast from these defects. The problem here is that many programs have been written for computers that now only exist in museums, by researchers who became professional programmers and never saw a TEM image again.

The first program to attempt the task of simulating two-dimensional images (rather than line profiles) of planar defects is described in the book by Head et al. Two current software packages are CuFour and

TEMACI. CuFour is the subject of an entire chapter in the companion text; TEMACI incorporated the ideas from Comis that we'll refer to here. We will mention some of the features of these programs to help you select one, but leave the detailed descriptions to the appropriate manuals. The most important reason for using any program must be your desire to understand the contrast and thus characterize the defect.

These programs are tools to assist you toward the goal of quantitative analysis of diffraction contrast, but you always need the fully quantitative experimental data, too. Few TEM users have ever collected such data.

You need an accurate simulation of the image you see in the microscope. The fact that the image varies with depth, thickness, **g**-vector, etc., is actually to your advantage, since you then have many variables, all of which you must be able to measure to achieve a good match with your experimental image. From the point of view of quantitative analysis, a one-dimensional line (intensity) profile is as valid as a two-dimensional image. Of course, if you can compare the contrast in an image and a simulation point by point, then you can have much greater confidence in the matching. The two-dimensional simulated image is also more viewer-friendly!

A great advantage of more powerful computers is that you can also test the effect of specimen geometry more readily. Thus, for example, Viguier et al. showed, using the CuFour simulation package, that the rules for fringe contrast given by Gevers et al. will not work if the specimen is tilted such that it intersects the bottom of the foil above the point where it intersects the top! You can understand this situation more easily by looking at the specimen geometry shown in Figure 25.15.

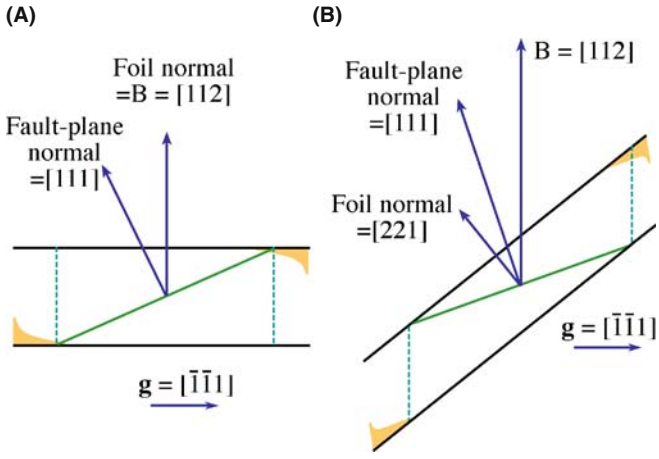

FIGURE 25.15. Many of the 'rules' for predicting the contrast from planar 'defects' make certain assumptions about the geometry of the defect relative to the surface of the specimen that may not always hold. The 'usual' situation is shown in (A) but the intersection of the planar defect with the upper specimen surface may be lower than the intersection with the bottom surface as in (B). This geometry can cause a reversal in the rules.

Image simulation tells us that $\mathbf{g}.\mathbf{R}$ must be > 0.02 to produce visible fringes, and you don't need to know the local structure at the planar defect when determining this condition. You could, in principle, detect smaller values of **R** by using larger **g**-vectors but in practice it then becomes more difficult to set up a well-defined diffraction geometry.

The next two sections are rather specialized and you may wish to leave them until much later, especially if you don't have access to a suitable program or until you are prepared to write your own. Do consult the key references and list of available programs in Section 1.6 before writing your own program. The subject is just as relevant to the topics of Chapters 26 and 27, but we include it in this chapter mainly because the analysis of planar defects is the most straightforward application.

25.12 THE GENERALIZED CROSS SECTION

Head et al. presented a method and a computer program for the computation of BF and DF images of line and planar defects. The source code is given in their book and is available from the WWW. You should note several important features of this program

- It uses the two-beam theory of electron diffraction.
- It uses the column approximation.
- The simulated image can be displayed as a halftone image rather than as intensity profiles.

This program was so successful, in part, because Head et al. were able to calculate the images quite quickly in spite of the fact that the computers available to microscopists were often not particularly powerful in ~1970. The calculations used a concept which they called the generalized cross section (GCS). (The GCS is not a scattering cross section, it is actually a slice through the specimen.) The GCS can be used when the displacement field, $u_{\mathbf{k}}$, satisfies the requirement that

$$u_{\mathbf{k}}(x, y, z) = u_{\mathbf{k}}(x, 0, z + cy) \qquad (25.34)$$

Here c is a constant and the foil is imagined to be laterally infinite. When this requirement is satisfied, the calculation of $u_{\mathbf{k}}$ is greatly simplified. One such situation is the important case where several dislocations and their associated fault planes are all parallel to one another. Then you only need to calculate the many-beam, Howie-Whelan equations on the plane $y = 0$. The displacement field for two columns y_1 and y_2 will only differ by a translation along the column, i.e., the z-direction. You don't want to repeat calculations you've already done; just calculate the image on a mesh in the x–y plane.

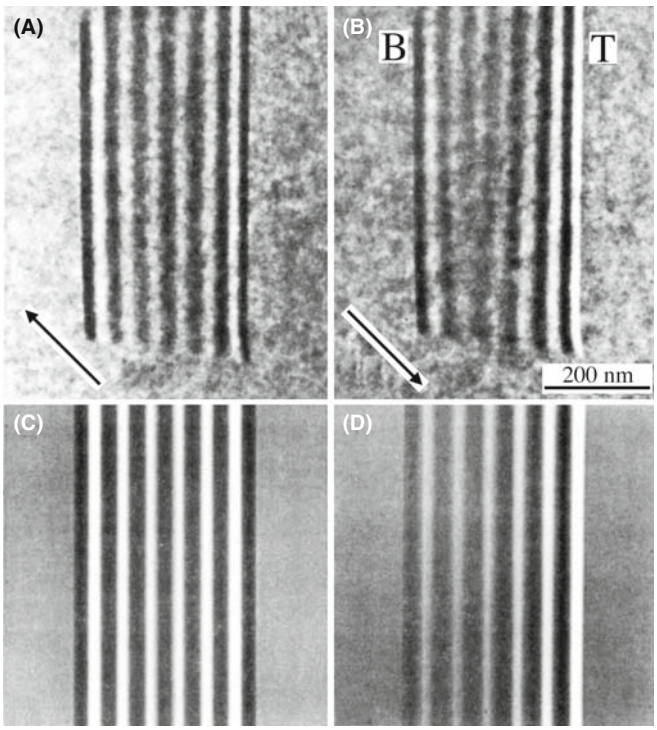

FIGURE 25.16. (A) Experimental BF image of an APB with $\mathbf{g} = 220$. (B) DF image of the same defect, $\mathbf{g} = \bar{2}20$. (C, D) Corresponding simulated images.

Examples of experimental and simulated images are shown in Figure 25.16. The simulation package used here (Comis again) was particularly attractive since it also performed elasticity calculations for simple defect configurations. It could simulate the effect of changing different parameters, and hence

- Change the accelerating voltage to see the extinction distances change.
- Change the absorption parameters to see the loss of SF-fringe contrast near the middle of the foil ($z = 0.5t$).
- Change the number of beams contributing to the image; how good is your two-beam assumption?
- Look at how reversing **g** changes the geometry of the image.
- Compare BF and DF as you vary the value of $\mathbf{s_g}$.

The Comis program ran on a Convex mini-supercomputer with an intelligent terminal, then on a Mac with OS6. Zhou used the concepts in the new and advanced package, TEMACI.

25.13 QUANTITATIVE IMAGING

One of the important applications of diffraction-contrast images is the detailed characterization of defects. With the improvements in the TEM, particularly in resolution and drift, we are now able to pay more attention to the fine structure of defects and this requires *quantitative* image analysis. In particular, we need to use the actual intensity levels in the image. One obstacle for quantitative analysis has been the uncertainty in the background-level intensity caused by inelastic scattering. As energy-filtered images become more widely available (see Chapter 37), we hope this problem will disappear. Direct digital recordings of the intensities, using a CCD camera are making quantitative analysis more tractable, eliminating uncertainties associated with the calibration of the response of the emulsion of the photographic film.

With these new applications of diffraction-contrast images in mind, improved simulation programs have become essential. An ideal program will be versatile, but user-friendly; it will allow us not only to calculate the image but also to give defect interaction geometries. In simulating images of crystal defects, you'll encounter several problems that are almost independent of one another. You must be able to do the following

- Define the geometry of the defects and of the specimen (the diffracting conditions).
- Calculate the displacement field associated with the defects.
- Propagate and scatter the electron beams throughout the foil (i.e., solve the Howie-Whelan equations).

We've already discussed the theoretical basis of the diffraction process, so we'll now illustrate some of the numerical methods which we can employ for different defect geometries. In Chapter 26, we'll consider other types of defects which may be analyzed, methods for defining them, and how we can calculate the displacement field.

25.13.A Theoretical Basis and Parameters

We'll use the Comis program as an example of the considerations that go into a simulation program. One message that you should certainly understand from this discussion is that you must be very cautious when using any program to simulate images. All such programs make assumptions and simplifications.

BLACK BOX

As always, when using the computer to simulate TEM images: beware of the black box. Don't automatically believe everything that comes out of it.

Comis was based on the Howie-Whelan dynamical theory of electron diffraction and thus neglects diffuse scattering but it could simulate without the column approximation. The basis of the approach used was given by Howie and Basinski.

- Use the deformable-ion approximation to describe how the crystal is influenced by the displacement field, **R**. In this model, the potential at **r** in the deformed crystal is assumed to be equal to the potential at the point **r** – **R**(**r**) in the perfect crystal. The model is good unless **R**(**r**) varies too rapidly.
- Extend the Howie-Whelan approach to many beams and avoid the column approximation.

The resulting equations are basically the same as those we derived in Chapter 13, so don't be put off by their appearance.

In treatments avoiding the column approximation, we include terms which allow for a variation in x and y: these terms were specifically excluded in Chapter 13.

The equations are now written as

$$\frac{\partial\phi_{\mathbf{g}}(r)}{\partial z} = \mathrm{i}\pi\sum_{\mathbf{h}}\left(\frac{1}{\xi_{\mathbf{g}-\mathbf{h}}}+\frac{\mathrm{i}}{\xi'_{\mathbf{g}-\mathbf{h}}}\right)\phi_{\mathbf{h}}e^{2\pi\mathrm{i}\left(\left(s_{\mathbf{h}}-s_{\mathbf{g}}\right)z-(\mathbf{h}-\mathbf{g})\,.\,\mathbf{R}\right)} - \theta_x\frac{\partial\phi_{\mathbf{g}}}{\partial x}-\theta_y\frac{\partial\phi_{\mathbf{g}}}{\partial y}+\frac{\mathrm{i}}{4\pi\chi_z}\left(\frac{\partial^2\phi_{\mathbf{g}}}{\partial x^2}+\frac{\partial^2\phi_{\mathbf{g}}}{\partial y^2}\right) \tag{25.35}$$

As usual, $\boldsymbol{\chi}$ is the incident-beam wave vector in vacuum, **g** is a particular diffraction vector, and **h** represents all the other possible diffraction vectors; you might like to compare this equation with equation 13.8! We have defined two new parameters to take account of the direction of the beam

$$\theta_x = \frac{(\boldsymbol{\chi}+\mathbf{g})_x}{\chi_z} \quad \text{and} \quad \theta_y = \frac{(\boldsymbol{\chi}+\mathbf{g})_y}{\chi_z} \tag{25.36}$$

The x–y plane in the reciprocal lattice contains the dominant reflections, and z is almost parallel to the incident beam. The number of beams you can include in the calculation is limited only by the capacity of your computer. The standard default for a program would be to select only beams on the systematic row. However, non-systematic beams can substantially influence your image, so it is useful if you can include sets of beams which are coplanar with the systematic row. We define the deviation of the crystal orientation from the exact Bragg condition by specifying the wave-vector components χ_x and χ_y; the latter applies when reflections outside the systematic row are included. Now we can calculate *all* the deviation parameters, $\mathbf{s}_{\mathbf{h}}$; there are many beams and each **s** can be different.

Each extinction distance $\xi_{\mathbf{g}}$ is defined as the ratio $\chi_{\mathbf{g}}/|U_{\mathbf{g}}|$, as usual with $U_{\mathbf{g}}$ being a Fourier component of the perfect-crystal potential. The Fourier components can be calculated from X-ray scattering factors, using the Mott expression. For most situations the scattering angle is small enough, so the X-ray scattering factors may, in turn, be calculated using the nine-parameter Gaussian fit given by Doyle and Turner.

You'll need to know the unit cell for your material and the Debye-Waller factor, B. Comis could then automatically calculate $\xi_{\mathbf{g}}$ using a built-in table of the Doyle-Turner parameters. You need to know B if you want to convert X-ray structure factors to electron structure factors (or vice versa) at a given temperature, or if you want to compare structure-factor measurements taken at different temperatures. When you calculate extinction distances, the Debye-Waller factors are essential to determine the effect of temperature.

DEBYE-WALLER FACTOR

B is related to the (mean-square) vibrational amplitude of an atom on a lattice site. It is a temperature-sensitive term.

Equation 25.35 is only valid if your crystal has a center of symmetry, otherwise we have to redefine $\xi_{\mathbf{g}}$. Simulations involving non-centrosymmetric crystals can be performed, but we have to replace the $\xi_{\mathbf{g}}$ and $\xi'_{\mathbf{g}}$ with complex quantities and then defining all the parameters is really difficult (see equations 14.2–14.8).

You can take account of absorption effects in the usual way by adding imaginary Fourier components, $U'_{\mathbf{g}}$ the absorption distances, $\xi'_{\mathbf{g}}$, are then defined as we discussed in Section 24.7. There are equations which a program can use to estimate the absorption distances, e.g., the linear relation $|U'_{\mathbf{g}}|/|U_{\mathbf{g}}| = a + b|\mathbf{g}|$, as suggested by Humphreys and Hirsch, or you could specify each individual absorption distance directly.

25.13.B Apparent Extinction Distance

The program developed by Head et al. was based on the two-beam approximation. The success of such calculations relies on the fact that the $\xi_{\mathbf{g}}$ may be replaced by an apparent extinction distance, $\xi^a_{\mathbf{g}} < \xi_{\mathbf{g}}$. This substitution compensates for scattering into beams that are not included in the two-beam calculation. The term $\xi^a_{\mathbf{g}}$ depends on t and must be estimated in each individual situation, e.g., by fitting the simulated image to your experimental image. For a quantitative image analysis it is important that you should have as few adjustable parameters as possible; using the many-beam program eliminates the need to use the parameter $\xi^a_{\mathbf{g}}$. Alternatively, you may determine $\xi^a_{\mathbf{g}}$ by comparing simulated thickness fringes calculated using many-beam and two-beam approximations.

25.13.C Avoiding the Column Approximation

Now you know we can perform simulations with or without the column approximation. With the column

approximation, you only keep the first term on the right-hand side of equation 25.35. The equations are reduced to a system of ordinary differential equations which the program must solve at each image point (x, y). In practice, the equation is solved on the nodes of a mesh (columns) using a fifth-order Runge-Kutta integration routine (which you, or the program, can look up when you need it). You need to choose the size and 'resolution' of the mesh. As we'll see in Chapter 27, there are situations where the column approximation will not be acceptable.

Without the column approximation, equation 25.35 gives us a system of coupled partial differential equations. The boundary conditions (at $z = 0$) can be generally written in the form

$$a_{\mathbf{g}}\phi_{\mathbf{g}} + b_{\mathbf{g}}\frac{\partial\phi_{\mathbf{g}}}{\partial x} = c_{\mathbf{g}} \qquad (25.37)$$

where we're ignoring changes in the y-dimension.

We can use fixed boundary conditions again following Howie and Basinski

- The foil is divided into thin slices of thickness Δz. You should not confuse this with the multislice method for lattice-image simulation which we'll see in Chapter 30; we are still using Howie-Whelan equations. Then, equation 25.35 is integrated, using the column approximation, through the first slice, i.e., from $z = 0$ to $z = \Delta z$, at all the mesh-points.
- The corrections to the column approximation, i.e., the terms containing derivatives with respect to x and y, are then evaluated by interpolation and included.
- The procedure is repeated until the exit surface of the foil is reached.

With this procedure, you are actually applying the column approximation to the outer boundary of the mesh. So, in equation 25.37 $a_{\mathbf{g}} = 1$, $b_{\mathbf{g}} = 0$, and $c_{\mathbf{g}} = \phi_{\mathbf{g}}$ at the initial surface. In order to avoid distortion of the image, we must choose the step size, Δz, carefully and be sure that the distance between columns (mesh size) is small enough (see Anstis and Cockayne).

25.13.D The User Interface

You'll want to run your program interactively so it should include commands which allow you to change parameters easily. Ideally, it will allow you to access each command through the keyboard using a menu. In Comis certain standard menus were available for special purposes. The user could also build (and save) menus interactively. This allowed all the relevant parameters and commands for a particular problem to be present within a single menu. At any time, all the commands were available through the keyboard.

Although typical simulations may be performed in a matter of seconds, many-beam calculations including several dislocations may require more CPU time. For this situation, Comis included a 'submit' command that would start a batch job based on your current data and parameters. Thus, the interactive mode could be used as a convenient way of submitting several jobs with varying parameter values.

For many problems, a purely visual comparison of experimental and simulated images is sufficient to allow you to interpret your image. In these situations, you can often find a $\xi^a_{\mathbf{g}}$ such that the simulations can be carried out with only two beams (à la Head et al.). However, since many parameters are involved in the image-matching process, it is best to eliminate as many unknown variables as possible. Many-beam calculations are even more important for quantitative analyses.

CHAPTER SUMMARY

The key points discussed in this chapter are

- We see contrast from planar defects because the translation, **R**, causes a phase shift $\alpha = 2\pi\mathbf{g}.\mathbf{R}$.
- In the two-beam case, we can derive analytical expressions to describe the contrast.
- We can use the scattering matrix method in the two-beam case and can readily extend it to more complicated multibeam situations.

Many different types of planar defect can be studied. You should be careful not to assume that all defects behave the same as SFs in fcc materials.

There is a direct relationship between the information in the images and that in the DPs, which you can understand using the concept of the relrod.

You need to understand how Bloch waves behave to explain why BF/DF pairs of images are not complementary and why the contrast from planar defects can disappear in the 'middle' of the image. The latter is a result of preferential absorption (really scattering) of certain Bloch waves.

We can now use computer modeling of diffraction-contrast images of planar defects to perform quantitative analysis and image matching.

REFERENCES

We suggest a few books or chapters of books for background reading. You'll realize that careers have been built on this topic. As usual, we also recommend that you read some of the original papers.

INTERFACES

Christian, JW 1975 *The Theory of Transformations in Metals and Alloys*, Part 1, 2nd edition, Pergamon Press New York.

Carter, CB and Norton, MG 2007 *Ceramic Materials* Springer New York. Chapters illustrating interfaces in ceramics.

Forwood, CT and Clarebrough, LM 1991 *Electron Microscopy of Interfaces in Metals and Alloys*, Adam Hilger New York. Invaluable for anyone studying interfaces by TEM.

Howe, JM 1997 *Interfaces in Materials: Atomic Structure, Thermodynamics and Kinetics of Solid-Vapor, Solid-Liquid and Solid-Solid Interfaces* Wiley New York.

Matthews, John Wauchope 1975, *Epitaxial Growth* Academic Press/Elsevier New York. Unfortunate use of 'epitaxial' instead of epitactic by a pioneer in the subject. (Yes, the father of Dave Matthews.)

Sutton, AP and Balluffi, RW 1995 *Interfaces in Crystalline Materials*, Oxford University Press New York.

Wolf, D and Yip, S, Eds. 1992 *Materials Interfaces, Atomic-level Structure and Properties*. Chapman and Hall New York.

THINKING ABOUT CONTRAST

The book by Head et al. (see Section 1.5) is the starting text for simulating diffraction-contrast images.

Amelinckx, S and Van Landuyt, J 1978 in *Diffraction and Imaging Techniques in Materials Science*, **1** and **2**, (Eds., S Amelinckx, R Gevers and J Van Landuyt), 2nd Ed., p. 107, North-Holland New York.

Anstis GR and Cockayne DJH 1979 *The Calculation and Interpretation of High-Resolution Electron Microscope Images of Lattice Defects* Acta Cryst. A**35**, 511–524.

Edington, JW 1976 *Practical Electron Microscopy in Materials Science*, Van Nostrand Reinhold New York. A classic practical guide but sometimes not suitable for modern TEMs.

Gevers R, Art, A and Amelinckx S 1963 *Electron Microscopic Images of Single and Intersecting Stacking Faults in Thick Foils – 1. Single faults* Phys. Stat. Sol. **3**, 1563–93.

Gevers R, Blank H and Amelinckx S 1966 *Extension of the Howie-Whelan Equations for Electron Diffraction to Non-Centro Symmetrical Crystals* Phys. Stat. Sol. **13**, 449–465. See this paper for discussion of imaginary extinction distances, $\xi'_{\mathbf{g}}$.

THE COLUMN APPROXIMATION

Howie A and Basinski ZS 1968 *Approximations of the Dynamical Theory of Diffraction Contrast* Phil. Mag. **17**, 1039–63. The non-column approximation paper.

Howie A and Sworn H 1970 *Column Approximation Effects in High Resolution Electron Microscopy Using Weak Diffracted Beams* Phil. Mag. **22**, 861–4. Example of a situation where the column approximation gives the wrong answer.

EXTINCTION DISTANCES

Doyle PA and Turner PS 1968 *Relativistic Hartree-Fock X-ray and Electron Scattering Factors* Acta Cryst. A**24**, 390–7.

Hashimoto, H, Howie, A and Whelan, MJ 1962 *Anomalous Electron Absorption Effects in Metal Foils: Theory and Comparison with Experiment* Proc. Roy. Soc. London A **269**, 80–103. Bloch waves and planar defects.

Hirsch PB, Howie A, Nicholson RB, Pashley DW and Whelan MJ 1977 *Electron Microscopy of Thin Crystals*, 2nd edition, p. 225, Krieger, Huntington, New York. Deduces equation 25.27.

Humphreys CJ and Hirsch PB 1968 *Absorption Parameters in Electron Diffraction Theory* Phil. Mag. **18**, 115–122.

Mott NF and Massey HSW 1965 *The Theory of Atomic Collisions*, 3rd Ed., Clarendon Press Oxford. Source of the Mott expression for X-ray scattering factors.

Taftø, J and Spence, JCH 1982 *A Simple Method for the Determination of Structure-Factor Phase Relationships and Crystal Polarity Using Electron Diffraction* J. Appl. Cryst. **15**, 60-4. Shows how to distinguish $\mathbf{g}$ and $\bar{\mathbf{g}}$ using CBED.

Yoshioka, H 1957 *Effect of Inelastic Waves on Electron Diffraction* J. Phys. Soc. Japan **12**, 618–628. See this paper for discussion of imaginary Fourier components, $U'_{\mathbf{g}}$.

SIMULATION

The original citation is the text by Head et al. (Section 1.5). It is still useful reading but needs a trip to the library.

Rasmussen, DR and Carter, CB 1991 *A Computer Program for Many-Beam Image Simulation of Amplitude-Contrast Images* J. Electron Microsc. Techniques **18,** 429–36. An idea of what we need in a user-friendly (Comis) program.
Rasmussen, DR, McKernan, S and Carter, CB 1991 *Rigid-Body Translation and Bonding Across {110} Antiphase Boundaries in GaAs* Phys. Rev. Lett. **66**, 2629–32.
Schaublin, R and Stadelmann, P 1993 *Method for Simulating Electron Microscope Dislocation Images* Mater. Sci. Engng. A**164**, 373–8. The paper describing CuFour.
Thölen AR 1970 *A Rapid Method for Obtaining Electron Microscope Contrast Maps of Various Lattice Defects* Phil. Mag. **22**, 175–182.
Thölen AR 1970 *On the Ambiguity Between Moiré Fringes and the Electron Diffraction Contrast from Closely Spaced Dislocations* Phys. Stat. Sol. (A) **2**, 537–550.
Viguier, B, Hemker, KJ and Vanderschaeve, G 1994 *Factors Affecting Stacking Fault Contrast in Transmission Electron Microscopy: Comparisons with Image Simulations* Phil. Mag. A**69**, 19–32.
Zhou, Z 2005 *Electron Microscopy and Elastic Diffuse Scattering of Nanostructures* D.Phil. Thesis, Oxford University. Zhongfu developed TEMACI.

THE COMPANION TEXT

Chapters on CuFour and more on TEMACI.

SELF-ASSESSMENT QUESTIONS

Q25.1 Describe the distinguishing features of the following interfaces: (a) phase boundary; (b) anti-phase boundary; (c) stacking fault.
Q25.2 What is α and for what values of α will planar defects not be seen?
Q25.3 Deduce the value of α for an fcc stacking fault.
Q25.4 A series of overlapping stacking faults show no contrast in the BF image. Explain how this could occur.
Q25.5 Which SF fringe is the same in both BF and DF images?
Q25.6 What interface gives complementary BF/DF fringes?
Q25.7 You can calculate the extinction distance. Can you confirm this value experimentally from an image?
Q25.8 What is the difference between a low-angle GB and a high-angle GB?
Q25.9 What does the concept of the scattering matrix allow to describe?
Q25.10 Why are BF/DF SF images usually not complementary?
Q25.11 Is the column approximation relevant to the study of planar defects?
Q25.12 Why might we see no contrast from the SF in the middle of the specimen even when we see fringes from the part close to each surface?
Q25.13 How does the planar defect affect the Bloch wave when it is close to the lower surface?
Q25.14 We describe SF contrast in terms of the inclination of the planar defect in the foil. When does this description clearly fail?
Q25.15 What does the term 'deformable-ion approximation' mean?
Q25.16 In deducing the propagation of Bloch waves in the presence of a SF, we use the tie line concept. What is the physical reason for using this concept in this situation?
Q25.17 Why do we recommend that you use the displaced-aperture DF approach for comparing BF and DF images?
Q25.18 Why is the displaced-aperture DF approach more useful today than in 1960?

TEXT-SPECIFIC QUESTIONS

T25.1 Consider Figure 25.5. At the far left of the lower image, the fringes are shifted. Explain this shifting using words and equations.
T25.2 Consider Figure 25.7 and if possible, the original paper. Confirm that the translation vector given in the text is correct. (Draw a larger diagram and deduce the direction and magnitude of **R**.)
T25.3 Consider Figure 25.8. Is this DF or BF and what is **g**? Explain your answer.
T25.4 In Figure 25.9, the contrast changes abruptly between regions that we might think of as 'grains.' Is this change real and why is it occurring?
T25.5 By considering Figure 25.10A and B, explain how the image will differ if the angle β is 30° or 150°.
T25.6 Is the shape of the sample in Figure 25.10c a perfect wedge? Discuss the reasons for your answer and the possible implications.
T25.7 Suggest a geometry for the anti-phase domain in Figure 25.8 using information from the fringes. Be as complete as possible.
T25.8 Explain why π fringes in Ni_3Al are so named.

T25.9 Extra challenge. By referring to the literature or otherwise, discuss the origin of the δ fringes in Figure 25.9. Are these fringes SF-type fringes? Is it coincidental that they end on arrays of dislocations? How would the fringes in CoO differ?

T25.10 Extra challenge. Explain the contrast in Figure 25.4 and relate them to one of the geometries. One difficulty you will encounter is identifying the first W fringe. Discuss why this is so.

T25.11 Sketch the possible SFs in Si for which the **g** vector is 131 and the beam direction is [2, 3, 11]. The planes on which the faults lie have been determined and are (111), (111), (111), and (111) for faults A, B, C, and D, respectively. How would you determine the nature of the SFs. Comment on why any intensity is observed for the faults on the $(\bar{1}\bar{1}\bar{1})$ and $(\bar{1}\bar{1}\bar{1})$ planes. (Adapted from Ian Robertson.)

T25.12 Consider a DP from two thin crystals and the corresponding moiré pattern. Both crystals are fcc structures. If you know that the magnification of the moiré pattern is 10^6 times and that the moiré pattern and the DP are correctly oriented with respect to each other, show how you would calculate the corresponding lattice parameters (a_1 and a_2) of the two fcc crystals. (Courtesy Matt Halvarson.)